Low-Field Magnetic Anisotropy of Sr2IrO4

Muhammad Nauman
Institute of Science and Technology (IST) Austria
Tayyaba Hussain
Kyungpook National University
Joonyoung Choi
Kyungpook National University
Nara Lee
Yonsei University
Young Jai Choi
Yonsei University
Woun Kang
Ewha Womans University
Younjung Jo (jophy@knu.ac.kr)
Kyungpook National University

Research Article

Keywords: Sr2IrO4, torque measurement, magnetic anisotropy, spin–orbit-coupled magnetic exchange interaction

Posted Date: August 25th, 2021

DOI: https://doi.org/10.21203/rs.3.rs-831500/v1

Version of Record: A version of this preprint was published at Journal of Physics: Condensed Matter on January 5th, 2022. See the published version at https://doi.org/10.1088/1361-648X/ac484d.

Low-field Magnetic Anisotropy of Sr_2IrO_4

Muhammad Nauman[a,b], Tayyaba Hussain[b], Joonyoung Choi[b], Nara Lee[c], Young Jai Choi[c], Woun Kang[d] and Younjung Jo[b*]

[a]Thermodynamics of quantum materials at the microscale laboratory, Institute of Science and Technology (IST) Austria, Klosterneuburg 3400, Austria

[b]Department of Physics, Kyungpook National University, Daegu 41566, Korea

[c]Department of Physics, Yonsei University, Seoul 03722, Korea

[d]Department of Physics, Ewha Womans University, Seoul 03760, Korea

Abstract

Magnetic anisotropy in strontium iridate (Sr_2IrO_4) is essential because of its strong spin-orbit coupling and crystal field effect. In this study, we investigated the detailed mapping of the out-of-plane (OOP) magnetic anisotropy in Sr_2IrO_4 for different sample orientations using torque magnetometry measurements in the low-magnetic-field region before the isospins are fully ordered. Dominant in-plane anisotropy was identified at low fields, confirming the *b* axis as an easy magnetization axis. Based on the fitting analysis of the strong uniaxial magnetic anisotropy, we observed that the main anisotropic effect arises from a spin–orbit-coupled magnetic exchange interaction that affects the OOP interaction. The interlayer exchange interaction results in additional anisotropic terms owing to the tilting of the isospins. Our results are relevant for understanding OOP magnetic anisotropy and provide a new way to analyze the effects of spin–orbit-coupling and interlayer magnetic exchange interactions. This study provides a new insight into the understanding of bulk magnetic, magneto-transport, and spintronic behavior of Sr_2IrO_4 for future studies.

Key words: Sr_2IrO_4, torque measurement, magnetic anisotropy, spin–orbit-coupled magnetic exchange interaction

*Corresponding author: jophy@knu.ac.kr

Introduction

Currently, 5d transition metal oxides have emerged as a captivating class of materials arising from strong spin–orbit or electron–lattice interactions [1-3]. This strongly interacting many-body system provides a possible platform for studying unique frustrations and anisotropic magnetic interactions [4-7]. The strong spin–orbit coupling (SOC) in these materials makes them most suitable for high-temperature superconductors, topological insulators, and devices with spintronics functionality [8]. Recent advances have opened a new paradigm for achieving spintronic functionality, namely antiferromagnetic spintronics [1,2,4-6,9-13]. Specifically, antiferromagnetic materials are of great interest because they have advantages such as no stray fields, insensitivity to magnetic fields, and fast antiferromagnetic (AFM) dynamics [14-16].

Strontium iridate (Sr_2IrO_4) is a representative 5d strongly-correlated electronic system. In a free Ir atom, the 5d states are degenerated because of the rotational symmetry of the atomic Hamiltonian. However, the crystal field removes the degeneracy and splits the 5d orbital. The 5d states are split into high-energy three-fold-degenerate (e_g) states and low-energy two-fold-degenerate (t_{2g}) states. The total effective orbital angular momentum (l_{eff}) of the t_{2g} state is 1, and the total spin sums up to 1/2. Because a strong SOC essentially entangles the spin and orbital momenta, a unique J_{eff} = 1/2 quantum state is formed by the pure spins and spatially anisotropic orbitals. This novel J_{eff} = 1/2 state can provide a comprehensive understanding of the correlation between the anisotropic magnetoresistance and magnetocrystalline anisotropy and help explore possible controllable AFM spintronics [16-21]. Magnetic anisotropy is a key phenomenon driven by a strong electron correlation. Magnetic anisotropy interactions and anisotropy energy are utilized in many industrial and technical fields [22]. The magnetocrystalline anisotropy in antiferromagnets arises from relativistic SOC. Microscopic observations have shown that the first nearest-neighbor basal-plane exchange constant is higher (60 meV) than the interlayer exchange constant (1 μeV), indicating a strong magnetic anisotropy [15,23,24].

The J_{eff} = 1/2 isospins in Sr_2IrO_4 can be modulated by applying an external magnetic field [5,15,19,25]. An in-plane canted AFM ordering arises below T_N ~ 240 K owing to the antisymmetric exchange interaction known as the Dzyaloshinskii–Moriya interaction (DMI) [26,27]. DMI competes with the symmetric Heisenberg interaction and favors spin-canting in an otherwise AFM system. A spin-canting angle of ~12° results in a net magnetic moment in each domain; however, AFM ordering along the *c* axis leads to a zero net magnetization [28]. The fascinating feature of Sr_2IrO_4 is that it exhibits both weak ferromagnetic (WFM) and AFM characteristics. The magnetic anisotropy and isospin reorientation strongly affect the electronic transport properties, making the material ideal for AFM-based spintronics functionality [19,29,30]. The magnetocrystalline contribution to the magnetic anisotropy in single-crystal Sr_2IrO_4 has been demonstrated based on torque magnetometry up to 9 T [3,29]. A two-fold sawtooth shape of the out-of-plane (OOP) rotation torque was evaluated. This strong OOP magnetic anisotropy shows that the magnetic easy axis is along the in-plane direction. In addition, the field-induced WFM order is attributed only to the in-plane component of the external magnetic field. We conducted a detailed study on the in-plane magnetic anisotropy in single-crystal Sr_2IrO_4 and found the *b* axis to be the easy axis of magnetization [22]. However, there is a lack of mapping of the explicit evolution of the isospins and the magnetic anisotropy for different OOP rotations. Moreover, it is essential to investigate the magnetic anisotropy of single-crystal Sr_2IrO_4 in the low-magnetic-field region before the isospins are fully ordered.

In this study, we verified OOP magnetic anisotropy before and after WFM transition and analyzed the *ac* and *bc* plane anisotropies separately. We present a comprehensive study of the low-field isospin interactions that generate in-plane anisotropy, where the static magnetic-domain structure is related to the orientation of the magnetic easy axis. Our work considers the various factors contributing to the anisotropy, such as the shape aniostropy, interfacial anisotropy, interlayer exchange coupling, and crystal symmetry, in the typical single-crystal Sr_2IrO_4 exhibiting strong SOC.

Results

Figure 1b shows the magnetization at 30 K when a magnetic field is applied along the *ab* plane. The magnetization gradually increases and saturates above a certain critical field at ~0.3 T with a small saturated moment [29]. A low degree of hysteresis with a negligible amount of residual net magnetization can be observed, indicating the WFM nature of Sr_2IrO_4 along the *ab* plane. There are two distinguishable domains: one with isospins along the *b* axis and the other with isospins along the *a* axis. A correlation exists between the isospin direction and the stacking pattern, which implies the presence of anisotropic interlayer coupling [30]. The

regions can be divided into a low field (<0.3 T) with a mixed-domain state and a high field (>0.3 T) with the WFM state. Figure 1c shows the various crystal orientations with respect to the reference axis marked by a red dotted line. ψ is a measure of the angle between the reference line and one specific corner of the crystal. To clarify the Ψ crystal orientation, a solid red line is displayed at one corner of the crystal. Because the SIO structure is tetragonal, we cannot distinguish between the a and b axes. Thus, we designated this corner as the a axis. We applied the angle-dependent torque $\tau(\theta)$ at $\Psi = 0°$, 25°, 90°, 120°, and 180°. By comparing $\tau(\theta)$ at $\Psi =$ 0° and 180°, as shown in Fig. 1d, we determined whether there is a difference in the magnetization strengths along the positive and negative a axes in the basal plane. Identical $\tau(\theta)$ values for $\Psi = 0°$ (solid line) and 180° (dotted line), including hysteresis around $\theta = 90°$, were observed. This confirms that the crystal was accurately placed on the cantilever without torsion. It represents a uniaxial magnetic behavior of the crystal along the in-plane direction. The sawtooth response of the torque in high magnetic fields is a dominant characteristic of Sr_2IrO_4 with a strong SOC. $\tau(\theta)$ vanishes at $\theta = 0°$ (180°) and $\theta = 90°$, indicating that the easy axis is either parallel or perpendicular to the crystal surface. As θ increases, the gradually increasing torque tends to change rapidly in the opposite direction near $\theta = 90°$, where the magnetic field passes through the c axis. This is characterized by a spin flop-like structure, indicating that the c axis is a hard magnetization axis and confirming the presence of an easy axis along the ab plane when the sample surface is parallel to the field direction, i.e., when $\theta = 0°$ (180°). This coincides with the reported AFM alignment of magnetic-domain magnetization along the a axis [31].

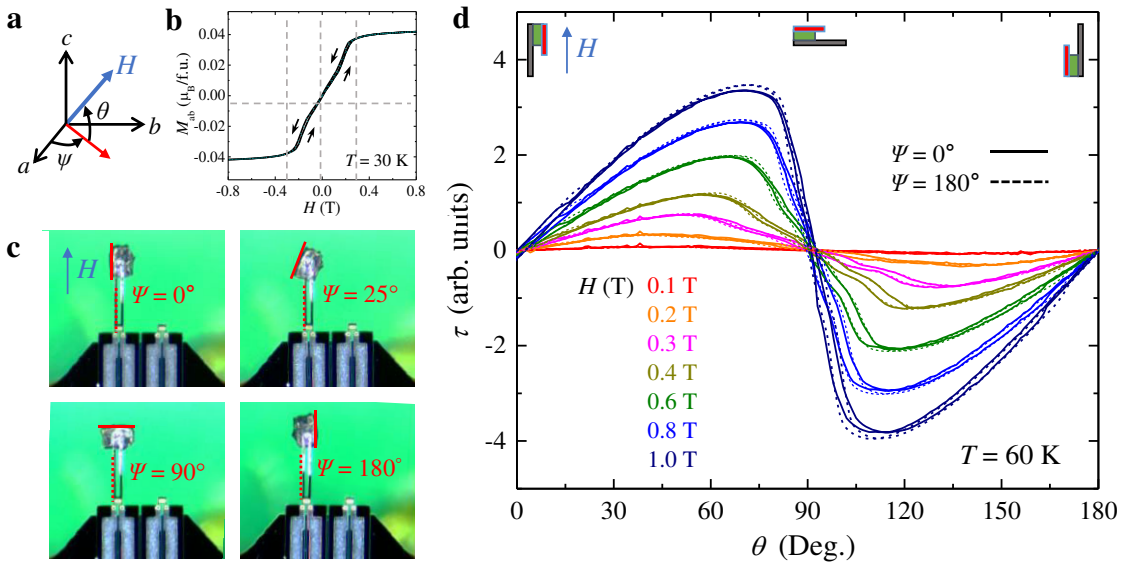

Figure 1: **a.** Definition of θ and ψ angles. **b.** Magnetization at 30 K under a magnetic field applied along the ab plane. **c.** Images of the crystal placed on the cantilever adjusted to various ψ angles. ψ is a measure of the angle between the reference line marked with red dotted and solid lines, at one corner of the crystal. **d.** $\tau(\theta)$ values for two opposite directions along the a axis, i.e., $\psi = 0°$ and 180°. The top sketch shows the alignment of the cantilever with the sample surface (red) parallel or perpendicular to the magnetic field.

Figures 2a and 2b show the $\tau(\theta)$ values for $\Psi = 0°$ (ac rotation), $\Psi = 90°$ (bc rotation), and $\Psi = 25°$ at $H = 0.1$ T and $H = 0.3$ T, respectively. At $H = 0.1$ T, the torque amplitude continuously increases when Ψ is varied from 0° to 90°, which can be explained by the increase in the magnetization strength. This dominant in-plane anisotropy at a low field becomes isotropic at higher fields. The magnetic field-dependent amplitude of τ/H at $\theta = 45°$, shown in Fig. 2c, is the relative amplitude of the magnetization. The difference in the amplitudes for different Ψ values solely arises from the difference in the magnetization strengths along the a and b axes, given that the c-axis magnetization is insignificant in Sr_2IrO_4 [29]. The hysteresis is significant in the low-H regime (H < 0.15),

reported as canted AFM-domain states [22] and disappears at 0.3 T, which is known as the field value where the WFM state is established [25,29]. The jump-like trait around $\theta = 90°$ is prominent only under *bc* rotation ($\Psi = 90°$). This difference in the torque curves may be due to the difference in the domain populations along the *a* and *b* axes.

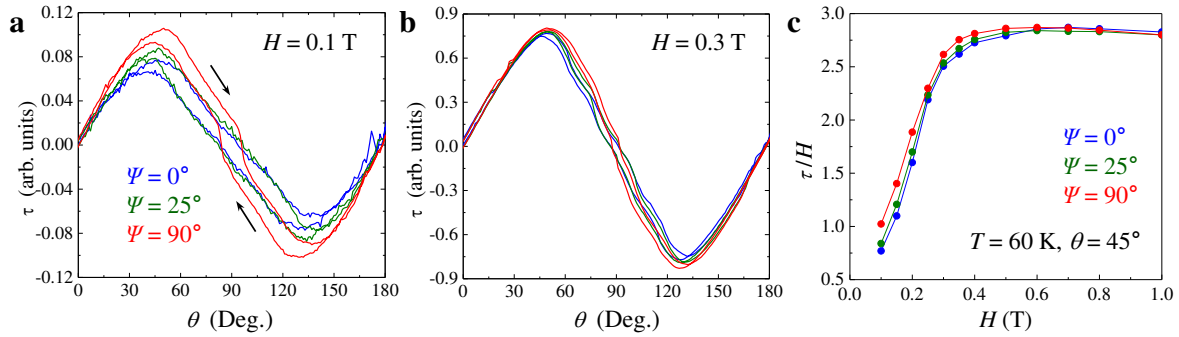

Figure 2: $\tau(\theta)$ values for three sample orientations ($\psi = 0°$, 25°, and 90°) at **a.** 0.1 T and **b**. 0.3 T. **c.** Amplitudes of the torque (τ/H) at $\theta = 45°$ for different ψ values.

Figure 3 shows the $\tau(\theta)$ for $\Psi = 0°$ under various magnetic fields at 60 K. The sin2θ angle dependence of the torque curves in the low-*H* regime is a characteristic of the linear response regime (inset of Fig. 3), while the deviation from this behavior at higher fields is direct evidence of the strong magnetic correlation. The sawtooth shape of the $\tau(\theta)$ curve at higher fields (>1 T) indicates the AFM ordering of the spins [3]. Generally, applying a high magnetic field that overcomes all the magnetic correlations helps restore the sin2θ dependence owing to the contribution of the Zeeman energy. However, in our case, the persistence of the sawtooth behavior above 0.3 T confirms the existence of a strong spin correlation [32].

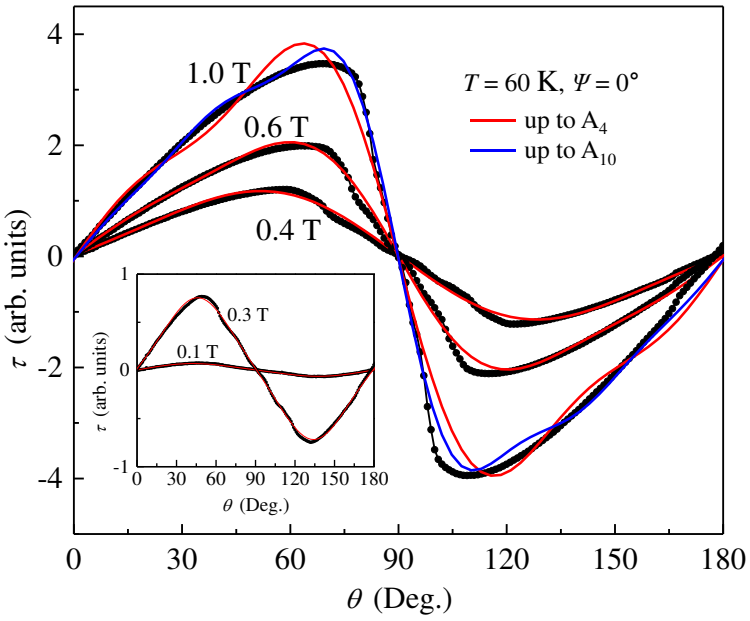

Figure 3: $\tau(\theta)$ for $\psi = 0°$ under various magnetic fields at 60 K. The red line fits the model. The inset shows $\tau(\theta)$ at 0.1 T and 0.3 T, low magnetic fields before WFM ordering. The red line and the blue line are the results of fitting on $\tau(\theta)$ at 1 T using equation (3) and equation (4), respectively.

To investigate the OOP magnetic anisotropies, we fitted the $\tau(\theta)$ curves. We introduced a mathematical model to determine the strong uniaxial magnetic anisotropy for multilayered systems [33]. Because of the layered structure of Sr_2IrO_4, which acts as a natural thin film, and electrons whose isospin orientation is strongly coupled to the pure spin magnetic moment in the plane, the model can be modified as follows:

The magnetic free energy can be written as $F = F_A + F_D + F_H$, which is a summation of the anisotropy energy (F_A), demagnetization energy (F_D), and free energy in the presence of an applied magnetic field (F_H), such that

$$F_A = k_1 \sin^2\theta + k_2 \sin^4\theta \quad (1a)$$
$$F_D = 2\pi M^2 \sin^2\theta \quad (1b)$$
$$F_H = -MH\cos(\varphi - \theta) \quad (1c)$$

Here, k_1 and k_2 are the second-order uniaxial anisotropy terms, and θ and φ are the angles of the magnetic field (H) and magnetization axis (M) from the ab plane, respectively.

Reducing the total energy of the system under equilibrium conditions $\left(\frac{\partial F}{\partial \theta} = 0\right)$ and rearranging the equations yield:

$$0 = (k_1 + k_2 + 2\pi M^2)\sin 2\theta - \frac{1}{2}k_2 \sin 4\theta - MH\sin(\varphi - \theta). \quad (2)$$

In equation (2), we set the coefficients of $\sin 2\theta$ and $\sin 4\theta$ as A_2 and A_4, respectively. The third term is the torque (τ); therefore, τ becomes

$$\tau = A_2 \sin 2\theta + A_4 \sin 4\theta. \quad (3)$$

A_2 characterizes an easy plane if $A_2 > 0$ and the easy axis if $A_2 < 0$. τ will be zero when $\varphi = \theta$, i.e., when H and M are parallel. For Sr_2IrO_4, the demagnetization energy contribution was negligible owing to the insignificant shape anisotropy [34]. Thus, it is easy to extract information regarding the magnetic anisotropy because of the crystal symmetry in the presence of H. The red lines in Fig. 3 indicate the fitting result obtained using equation (3). Up to 0.3 T, the fitting formula yields a relatively good fit; however, the higher the magnetic field, the worse the fitting. To obtain a more accurate fitting curve, we added a higher-order anisotropy term to equation (3) as follows.

$$\tau = A_2 \sin 2\theta + A_4 \sin 4\theta + A_6 \sin 6\theta + A_8 \sin 8\theta + A_{10} \sin 10\theta. \quad (4)$$

The blue line indicates the result of fitting on $\tau(\theta)$ at 1 T using equation (4); in this case, the result is better but still not perfect.

Anisotropic magnetism can be estimated by comparing the amplitude of the nth-fold symmetric contribution, A_n (see Fig. 4). Two-fold symmetry contributions are the major contributions, as evident from the $\tau(\theta)$ curves. The amplitude of $\sin 2\theta$ (A_2) is positive at all magnetic fields, confirming that the anisotropy in Sr_2IrO_4 is an easy-plane type. A_2 is higher for $\Psi = 90°$ than for $\Psi = 0°$, indicating that the bc plane is an easy plane. A_2 gradually changes in the low-H regime and then increases linearly. This demonstrates weak spin responses because of the lower Zeeman energy contributions in the low-H regime. The nonsaturation of all A_n up to 1 T is because the applied magnetic field is insufficient to overcome the high anisotropic energy barrier between the ab plane and the c axis. A_2 encodes all possible anisotropy contributions, including both intrinsic characteristics, such as the crystal structure and magnetic interaction, and extrinsic characteristics, such as the shape and surface effects. The extrinsic contributions are insignificant in Sr_2IrO_4, as reported in the literature because of the small crystal dimensions (0.1 mm) and minor spin-glass phenomena [34]. Thus, the main anisotropic effect arises from a spin–orbit-coupled magnetic exchange interaction. The higher-order term is essential in systems exhibiting interfacial anisotropy. This interfacial anisotropy is most common in thin magnetic films. In our OOP measurements of Sr_2IrO_4, interfacial anisotropy cannot be a premise for total magnetic anisotropy; however, it cannot be excluded.

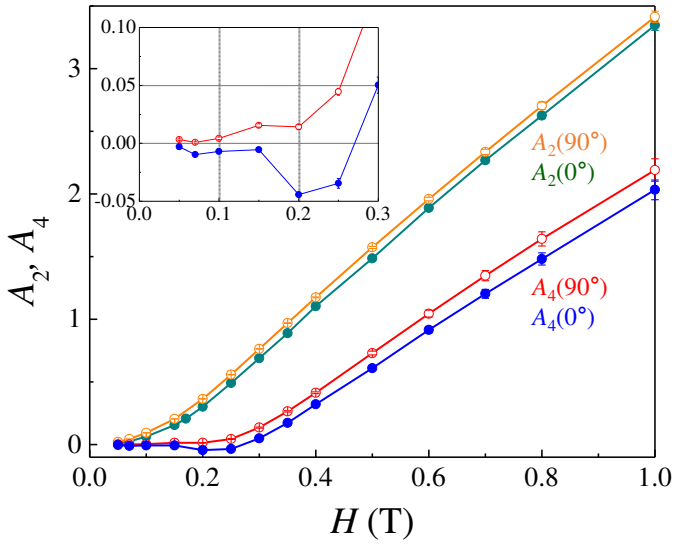

Figure 4: Amplitude of the nth-fold symmetric contribution, A_n (n = 2, 4) obtained using equation (3) at $\Psi = 0°$ and $\Psi = 90°$.

Nonzero A_4 appears near the high-field regime (H > 0.3 T) when $\tau(\theta)$ deviates from the sin2θ pattern. Since SIO has weak OOP magnetic coupling or magnetic exchange interaction [15,31], nonzero A_4 pertains to the weakly coupled regions whose high prospect is in the OOP anisotropy measurements. In the low-H regime (H < 0.3 T), A_4 is negative for $\Psi = 0°$ and positive for $\Psi = 90°$, as shown in the inset of Fig. 4. The positive value of A_2 (A_2 > 0) and negative value of A_4 (A_4 < 0) for $\Psi = 0°$ (ac rotation) can be interpreted as the canted state, indicating AFM ordering along the a axis in the ab plane [31]. It is also associated with a metamagnetic transition, where the system first becomes AFM_a (AFM ordering along the a axis) and then transitions to an FM state above 0.3 T by applying a magnetic field along the in-plane [35]. Because the b axis is an easy axis of magnetization, no such A_4 < 0 can be observed for $\Psi = 90°$ (bc rotation) in the absence of any metamagnetic transition. Coupling along the c axis (J_c) is weaker than in-plane coupling (J_{ab}) [15]. Because there is a correlation between the isospin direction and the stacking pattern, there is anisotropic interlayer coupling depending on the field applied along the a axis of the b axis. This partial fluctuation in the first nearest-layer exchange (J_{1c}) following the staggering of the isospins in the adjacent layers may also cause this variation in A_4 below 0.3 T. The shift toward positive values above 0.3 T is based on the fact that the FM state cannot be realized by applying H along the hard axis, i.e., c axis. The application of a high field along the OOP direction will result in an induced magnetization along the c axis owing to the tilting of the isospins. Such slight tilting of the isospins generates additional anisotropic terms (A_4 and higher-order parameters) and provides important information about the system. This will lead to the emergence of higher orders at fields >0.3 T, and off-diagonal interactions will lead to a sawtooth behavior in $\tau(\theta)$. The reason for the increase in the bifurcation of the A_4 curves for ac and bc rotations in the high-field regime remains unknown.

Discussion

Based on torque magnetometry measurements of single-crystal Sr_2IrO_4 for different OOP rotations, we identified the magnetic easy axis along the ab plane, which coincides with the AFM alignment of the magnetic domain along the a axis. This dominant in-plane anisotropy at low fields with a mixed-domain state becomes isotropic in higher fields with the WFM state. The sawtooth response of the torque in a high magnetic field is characterized by a spin flop-like change when the field passes through the c axis, which is a hard magnetization axis. This deviation from the sin2θ dependence of the torque is direct evidence of a strong magnetic correlation. By performing a fitting analysis of the strong uniaxial magnetic anisotropy, we compared the amplitudes of the two-fold (A_2) and four-fold (A_4) symmetric contributions. The higher value of A_2 for bc rotation than for ac rotation indicates that the bc plane is an easy plane. The nonzero value of A_4 in the high-field regime is attributed to a weakly coupled interlayer direction along with a slight tilting of the isospins generates additional anisotropic terms. In-plane magnetic anisotropy causes the OOP exchange interaction that results in differences in ac- and bc-plane anisotropies. Our results provide a complete mapping of OOP magnetic anisotropy,

verifying that major anisotropic effects arise from spin–orbit-coupled magnetic exchange interactions. The results are important in understanding the GMR-like effect in single crystal Sr_2IrO_4 reported recently [15] and provide an insight into OOP magnetic anisotropy in the low (< 1 T) magnetic field regime.

Methods

Sr_2IrO_4 crystals were prepared using a flux method with $SrCl_2$ as the flux [3]. Crystallinity was confirmed using X-ray diffraction measurements. Single-crystal Sr_2IrO_4 was mounted on a piezoresistive cantilever with a crystallographic *c* axis perpendicular to the plane of the lever. The change in the torque was measured by the change in the resistance of the piezo material comprising a Wheatstone bridge circuit [3,22]. This is a nondestructive and reliable technique for detecting spin canting and domain magnetization. The magnetic field direction with respect to the crystal axis was controlled using a rotator. We applied the OOP angular-dependent torque of Sr_2IrO_4, i.e., $\tau(\theta)$, for various crystal orientations by varying ψ. Here, θ is the angle between the applied magnetic field and the *ab* plane, and ψ is the crystal orientation with respect to the reference axis in the in-plane direction (see Fig. 1a).

Data availability: No datasets were generated or analyzed during the current study.

References:

1 Zwartsenberg, B. *et al.* Spin-orbit-controlled metal–insulator transition in Sr_2IrO_4. *Nature Physics* **16**, 290-294 (2020).

2 Ye, F., Hoffmann, C., Tian, W., Zhao, H. & Cao, G. Pseudospin-lattice coupling and electric control of the square-lattice iridate Sr_2IrO_4. *Physical Review B* **102**, 115120 (2020).

3 Hong, Y. *et al.* Large magnetic anisotropy in canted antiferromagnetic Sr_2IrO_4 single crystals. *Physical Review B* **93**, 094406 (2016).

4 Chen, C. *et al.* Persistent insulating state at megabar pressures in strongly spin-orbit coupled $Sr2IrO_4$. *Physical Review B* **101**, 144102 (2020).

5 Bertinshaw, J., Kim, Y., Khaliullin, G. & Kim, B. Square Lattice Iridates. *Annual Review of Condensed Matter Physics* **10**, 315-336 (2019).

6 Souri, M. *et al.* Optical signatures of spin-orbit exciton in bandwidth-controlled Sr_2IrO_4 epitaxial films via high-concentration Ca and Ba doping. *Physical Review B* **95**, 235125 (2017).

7 Kim, B., Kim, B. H., Kim, K. & Min, B. Substrate-tuning of correlated spin-orbit oxides revealed by optical conductivity calculations. *Scientific reports* **6**, 27095 (2016).

8 Hermanns, M., Kimchi, I. & Knolle, J. Physics of the Kitaev model: Fractionalization, dynamic correlations, and material connections. *Annual Review of Condensed Matter Physics* **9**, 17-33 (2018).

9 Jackeli, G. & Khaliullin, G. Mott insulators in the strong spin-orbit coupling limit: from Heisenberg to a quantum compass and Kitaev models. *Physical review letters* **102**, 017205 (2009).

10 Schaffer, R., Lee, E. K.-H., Yang, B.-J. & Kim, Y. B. Recent progress on correlated electron systems with strong spin–orbit coupling. *Reports on Progress in Physics* **79**, 094504 (2016).

11 Rau, J. G., Lee, E. K.-H. & Kee, H.-Y. Spin-orbit physics giving rise to novel phases in correlated systems: Iridates and related materials. *Annual Review of Condensed Matter Physics* **7**, 195-221 (2016).

12 Winter, S. M. *et al.* Models and materials for generalized Kitaev magnetism. *Journal of Physics: Condensed Matter* **29**, 493002 (2017).

13 Natori, W. M., Moessner, R. & Knolle, J. Orbital magnetic field effects in Mott insulators with strong spin-orbit coupling. *Physical Review B* **100**, 144403 (2019).

14 Maniv, E. *et al.* Antiferromagnetic switching driven by the collective dynamics of a coexisting spin glass. *Science advances* **7**, eabd8452 (2021).

15 Wang, H. *et al.* Giant anisotropic magnetoresistance and nonvolatile memory in canted antiferromagnet Sr_2IrO_4. *Nature communications* **10**, 2280 (2019).

16 Zhou, H., Xu, Y.-Y. & Zhou, S. Electron Correlations, Spin-Orbit Coupling, and Antiferromagnetic Anisotropy in Layered Perovskite Iridates Sr_2IrO_4. *Communications in Theoretical Physics* **70**, 081 (2018).

17 Louat, A. *et al.* ARPES study of orbital character, symmetry breaking, and pseudogaps in doped and pure Sr_2IrO_4. *Physical Review B* **100**, 205135 (2019).

18 Khalyavin, D. & Lovesey, S. Anapole correlations in Sr_2IrO_4 defy the j_{eff}=1/2 model. *Physical Review B* **100**, 224415 (2019).

19 Lu, C. & Liu, J. M. The J_{eff}= 1/2 Antiferromagnet Sr_2IrO_4: A Golden Avenue toward New Physics and Functions. *Advanced Materials* (2019).

20 Calder, S., Pajerowski, D. M., Stone, M. B. & May, A. F. Spin-gap and two-dimensional magnetic excitations in Sr_2IrO_4. *Physical Review B* **98**, 220402 (2018).
21 Hussain, T. *et al.* Pressure-induced metal–insulator transitions in chalcogenide $NiS_{2-x}Se_x$. *Physica B: Condensed Matter* (2017).
22 Nauman, M. *et al.* In-plane magnetic anisotropy in strontium iridate Sr_2IrO_4. *Physical Review B* **96**, 155102 (2017).
23 Kim, J. *et al.* Magnetic excitation spectra of Sr_2IrO_4 probed by resonant inelastic X-ray scattering: establishing links to cuprate superconductors. *Physical Review Letters* **108**, 177003 (2012).
24 Fujiyama, S. *et al.* Two-dimensional Heisenberg behavior of J_{eff}=1/2 isospins in the paramagnetic state of the spin-orbital Mott insulator Sr_2IrO_4. *Physical review letters* **108**, 247212 (2012).
25 Jeong, J. *et al.* Magnetization Density Distribution of Sr_2IrO_4: Deviation from a Local j_{eff}=1/2 Picture. *Physical Review Letters* **125**, 097202 (2020).
26 Kim, J.-W. *et al.* Controlling symmetry of spin-orbit entangled pseudospin state through uniaxial strain. *Physical Review B* **102**, 054420 (2020).
27 Liu, P. *et al.* Anisotropic magnetic couplings and structure-driven canted to collinear transitions in Sr_2IrO_4 by magnetically constrained noncollinear DFT. *Physical Review B* **92**, 054428 (2015).
28 Samanta, K., Tartaglia, R., Kaneko, U., Souza-Neto, N. & Granado, E. Anisotropic lattice compression and pressure-induced electronic phase transitions in Sr_2IrO_4. *Physical Review B* **101**, 075121 (2020).
29 Lee, N. *et al.* Antiferromagnet-Based Spintronic Functionality by Controlling Isospin Domains in a Layered Perovskite Iridate. *Advanced Materials*, 1805564 (2018).
30 Meyers, D. *et al.* Magnetism in iridate heterostructures leveraged by structural distortions. *Scientific reports* **9**, 4263 (2019).
31 Porras, J. *et al.* Pseudospin-lattice coupling in the spin-orbit Mott insulator Sr_2IrO_4. *Physical Review B* **99**, 085125 (2019).
32 Modic, K. A. *et al.* Robust spin correlations at high magnetic fields in the harmonic honeycomb iridates. *Nature communications* **8**, 1-5 (2017).
33 Poulopoulos, P., Flevaris, N., Krishnan, R. & Porte, M. Methods of determining magnetization and uniaxial anisotropy of multilayers by means of torque magnetometry. *Journal of applied physics* **75**, 4109-4113 (1994).
34 Fruchter, L., Colson, D. & Brouet, V. Magnetic critical properties and basal-plane anisotropy of Sr_2IrO_4. *Journal of Physics: Condensed Matter* **28**, 126003 (2016).
35 Zhang, H. *et al.* Comprehensive Electrical Control of Metamagnetic Transition of a Quasi-2D Antiferromagnet by In Situ Anisotropic Strain. *Advanced Materials* **32**, 2002451 (2020).

Acknowledgments

Y.J. was supported by the National Research Foundation of Korea (NRF) (Grant Nos. NRF-2018K2A9A1A06069211 and NRF-2019R1A2C1089017). The work at Yonsei was supported by the NRF (grant Nos. NRF-2017R1A5A1014862 (SRC program: vdWMRC center), NRF-2019R1A2C2002601, and NRF-2021R1A2C1006375). W.K. acknowledges the support by the NRF (Grant Nos. 2018R1D1A1B07050087, 2018R1A6A1A03025340).

Author Contributions: M.N., Y.J.C., and Y.J designed the experiments. N.L. and Y.J.C. synthesized the single crystals. M.N., T.H., J.C., W.K., and Y.J. carried out measurements of physical properties. M.N. and Y.J. analyzed the data and prepared the manuscript. All the authors have read and approved the final version of the manuscript.

Competing Interests: The authors declare no competing interests.

Figure Legends

Figure 1: **a.** Definition of θ and ψ angles. **b.** Magnetization at 30 K under a magnetic field applied along the *ab* plane. **c.** Images of the crystal placed on the cantilever adjusted to various ψ angles. ψ is a measure of the angle between the reference line marked with red dotted and solid lines, at one corner of the crystal. **d.** $\tau(\theta)$ values for two opposite directions along the *a* axis, i.e., ψ = 0° and 180°. The top sketch shows the alignment of the cantilever with the sample surface (red) parallel or perpendicular to the magnetic field.

Figure 2: $\tau(\theta)$ values for three sample orientations (ψ = 0°, 25°, and 90°) at **a.** 0.1 T and **b**. 0.3 T. **c.** Amplitudes of the torque (τ/H) at θ = 45° for different ψ values.

Figure 3: $\tau(\theta)$ for $\psi = 0°$ under various magnetic fields at 60 K. The red line fits the model. The inset shows $\tau(\theta)$ at 0.1 T and 0.3 T, low magnetic fields before WFM ordering. The red line and the blue line are the results of fitting on $\tau(\theta)$ at 1 T using equation (3) and equation (4), respectively.

Figure 4: Amplitude of the *n*th-fold symmetric contribution, A_n (n = 2, 4) obtained using equation (3) at $\Psi = 0°$ and $\Psi = 90°$.